STM JOURNALS

International Journal of
Bioinformatics and
Computational Biology

Volume 1, Issue 2, 2023
DOI (Journal): 10.37628/IJBCB
July–December

https://journals.stmjournals.com/ijbcb/

Research IJBCB

A Structure-based Design Approach to *Catharanthus roseus* Phytoconstituents as Potential Inhibitors of B-Cell Lymphoma 6 Protein

Shahid Attar[1,*], Samiksha Bhor[2]

Abstract

Objectives: *Lymphoma is a cancerous disease. It develops into millions of people worldwide. Identify the naturally active compounds from Catharanthus roseus, they have multiple values in the medicinal field of Siddha, and Indian Ayurveda are used as a disease-preventing agent. Drug illness prediction, toxicity prediction, statistical information, molecular docking, as well as absorption, distribution, metabolism, and excretion (ADME) analysis are used to predict the fit ligand as a drug.* ***Methods:*** *The database of protein data bank (PDB) was used to retrieve the BCL6 protein and its chains after the purification. The poor binding affinity of ligands with target protein was removed, ADMET analysis and Swiss-ADME lab webserver were used for drug-likeness analysis, and molecular docking is done with the PyRx.* ***Results:*** *The dihedral angles Φ and ψ combination in the backbone of protein is shown in the Ramachandran plot analysis. The five compounds of C. roseus have a potential binding affinity with BCL6 found in molecular docking. ADMET profile and docking interaction showed five compounds Perivine, Alstonine, Quercetin, 16-Methoxytabersonine, and Vindolininol are possess the properties of the drug and safe to use.* ***Conclusion:*** *The previous and present studies suggest that Perivine, Alstonine, Quercetin, 16-Methoxytabersonine, and Vindolininol could inhibit the chain A, B, and C of BCL6 protein and have significant affinity binding. The therapeutic strategies against B-cell lymphoma interpreted based on molecular binding and interaction.*

Keywords: *Catharanthus roseus*, B-cell lymphoma, Cancer, Phytocompound, BCL6, Auto-docking, ADMET analysis.

INTRODUCTION

***Author for Correspondence**
Shahid Attar
E-mail: shahidattar0099@gmail.com

[1]Student, Department of Bioinformatics, BioNome, Bengaluru, Karnataka, India
[2]Bioinformatics Associate, Department of Biotechnology, BioNome, Bengaluru, Karnataka, India

Received Date: May 9, 2023
Accepted Date: May 31, 2023
Published Date: June 30, 2023

Citation: Shahid Attar, Samiksha Bhor. A Structure-based Design Approach to *Catharanthus roseus* Phytoconstituents as Potential Inhibitors of B-Cell Lymphoma 6 Protein. International Journal of Bioinformatics and Computational Biology. 2023; 1(2): 14–34p.

Lymphomas are the cancer of the lymphatic system divided into Non-Hodgkin (NHL) and Hodgkin (NL), where approximately 90% and 10% of illnesses are observed. B-cell, T-cell, and NK-cell types observed in NHL and NL were divided into classical and nonclassical types. Diffuse large B-cell lymphoma, follicular lymphoma, extranodal marginal zone lymphoma of mucosa-associated lymphoid tissue, mantle cell lymphoma, and Burkitt lymphoma are types of B-cell lymphoma [1]. The effective humoral immune response depends on the BCL6 protein interacting with transcriptional factors, and signaling mediators. The BCL6 helps B-cell hyper somatic mutation and development in the germinal center (GC) [2].

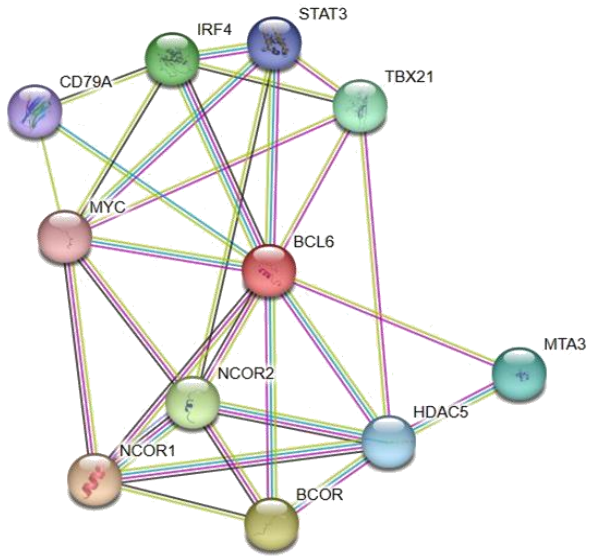

Figure 1. Network and interactions of BCL6 protein obtained in STRING 11.5.

BCL6 is involved in multiple pathways including Phosphatidylinositol 3- kinase/mammalian target rapamycin (PI3k/mTOP) pathway [3], the B-cell receptor/spleen tyrosine kinase (BCR/syk) pathway [4], protein kinase C- beta (PKC-B) pathway [5] were major paths. Serine/threonine protein kinase [6], deregulation of Ras/Raf/MAPK/ERK pathway [7], and coactivation of NF-kB and Notch signaling [8]. Cancer cells can have high expression of clusters of differentiation (CD) such as CD20, CD21, CD22, CD30, CD45, CD79a [9], and lactate dehydrogenase [10].

BCL6 has networked with STAT3, IRF4, TBX21, CD79A, MYC, MTA3, NCOR1, NOCOR2, BCOR, and HDAC5, as shown in Figure 1. Signal transducer and activator of transcription 3 (STAT3) shows the positive expression of BCL6 [11] and responsible for the decrease berg cell and increase the T-cell and plasma cell [12]. INF-regulatory factor 5 (IRF5) is responsible for express plasma cell maturation protein Blimp-1 to induce short- or long-lived plasma cells and increase $CD19^{+}$ [13]. Interleukin 4 is produced by signaling T-Box Transcription Factor 21 (TBX21) to T-cells [14] and indirectly increases the BCL6 [15]. CD79A is expressed as an antigen in Mantle cell lymphoma by CCND1 (Cyclin D1) from the Cyclin D protein family [16]. Double-hit (DH) lymphomas are associated with Burkitt lymphoma type of aggressive lymphoma by MYC proto-oncogene [17]. Metastasis-associated protein 3 (MTA3) is a master regulator of plasma cells by expressing BCL6 and Blimp-1 [18]. B-cell corepressor (BCOR) and nuclear receptor corepressor 1 and 2 (NCOR1, NOCR2) multifunctional complex bound to BCL6 gene promoter [19]. Histone deacetylase 5 (HDAC5) suppresses the BCL6 function [20].

Catharanthus roseus Linn also known as Madagascar periwinkle or Sadabahar belongs to the family Apocynaceae. More than 200 alkaloids have medicinal properties. Secondary metabolites are present in leaves (vinblastine, vindoline, catharanthine, and vincristine) as well as stem and roots (reserpine, ajmalicine, serpentine, vindoline, tabersonine, catharanthine, and horhammericine) [21].

MATERIALS AND METHODS

Selection and Preparation of the Target Protein

AutoDock is a popular program for the analysis of receptor-ligand docking [22]. The three-dimensional structure of the target B-cell Lymphoma (BCL6) BTB domain (Homo 2-mer) was downloaded in PDB format from the RCSB Protein Data Bank (https://www.rcsb.org/) [23]. Visualized

the protein by using the software Discovery Studio 2021 v21.1.0.20298 (BIOVIA) and water molecules, ions, and ligands were removed. The modified protein was saved in PDB format for further AutoDock analysis [24].

Selection and Preparation of the Ligand

The phytochemical compounds of the *C. roseus* plant (flower and leave), as shown in Figure 2 [25]. Compounds extracts were considered for the molecular docking study. The phytocompounds selected from the IMPPAT webserver (https://cb.imsc.res.in/imppat/) have been listed as in the medicinal plants and 3D structure downloaded in the structure-data file (SDF) format from PubChem (http://pubchem.ncbi .nlm.nih.gov/). Canonical SMILES data of phytocompound was collected for the ADMET analysis [26].

Molecular Docking

Biomedical research is used to discover drugs for improving the health of the population. The chemical compounds (small molecules) produced naturally in plants, might be used as a drug for the treatment of diseases. BCL6 protein target-based screening compounds were tested with purified macromolecules to find leads of compounds. The virtual molecular screening was carried out using the AutoDock Vina with the help of the PyRx Virtual Screening Tool version Python Prescription 0.8. Phytochemicals should be converted into a PBDQT file format before using the virtual screening docking [27]. The grid center for purified BCL6 homo2-mer included chains A and B of PDB ID 1R28 protein was set X = 17.830 Y = -14.691 Z = -11.7689 and dimensions (Angstrom) at X = 46.3529, Y = 45.6205, and Z = 64.1666. The grid center set for purified chain A of BCL6 homo2-mer (PDB ID 1R28) X = -19.731, Y = -19.712, and Z = -1.4562, the dimensions X = 42.4292, Y = 35.5845, and Z = 49.3924. The grid center set for purified chain B of BCL6 homo2-mer (PDB ID 1R28) X = -15.930, Y = -9.6713, and Z = -22.0815, and the dimensions X = 45.07773, Y = 42.4481, and Z = 57.4296. The docking results obtained in binding energy (Kcal/mol) of phytochemicals interactions with the protein were compiled in a CVS file format. The affinity binding score was more negative and chosen for further analysis, the ligand out pdbqt file was downloaded in PDB file format from PyRx and was submitted to BIOVIA software to observe the structure and interaction between ligands and target protein.

In Silico ADME Analysis

Absorption, Distribution, Metabolism, Extraction, and Excretion parameter were used for the pharmacokinetics study by evaluating the ligand using Swiss ADME (http://www.swissadme.ch/ index.php). The canonical SMILES of ligands were obtained in PubChem (http://pubchem.ncbi.nlm .nih.gov/) and used for Swiss ADME analysis [28]. They check drug ability in the discovery of drugs by evaluating multiple parameters, such as physiological properties, biological effects, permeability, toxicity, and bioavailability. Lipinski and Co-workers correlated values preferred, as shown in Table 1.

Figure 2. *Catharanthus roseus.*

Table 1. Lipinski rule parameters.

Property	Optimal range
Molecular weight	<500 Daltons
MlogP	<4.15
H Donors	<5
H acceptors	<10
Molecular refractivity	40–130

Molecular weight, partition coefficient (MlogP), Hydrogen donor, Hydrogen acceptor, molecular refractivity, polar surface area, number of rotatable bonds, solubility, permeability, bioavailability, and synthetic accessibility were analyzed according to Lipinski parameters. Five rules of Lipinski were considered for checking a drug illness [29].

Physiochemical Properties

The size (molecular weight), Saturation (Sp3 hybridization or fraction Csp3), flexibility (rotational bond), polarity (a topological polar surface area or TPSA), Lipophilicity (xLogP) were checked in physiochemical properties, as shown in Table 2.

Toxicity Analysis

Protox webserver published in the year 2014, the toxicity of the drug was checked by inserting SMILES into ProTox-II. Drug toxicity is an important factor in drug discovery to be predicted as a toxic or less-toxic or non-toxic drug. Protox radar was generated from the data on acute toxicity, organ toxicity, toxicological endpoints, toxicological pathways, and toxicity targets. It is a better computational method to predict than other software. It is most commonly used by toxicologists [30]. The toxicity of the phytochemical properties was predicted by the ProTox-II tool. The lethal dose (LD50) and predicted class of toxicity. LD_{50} were classified into class I, II, III, and IV, as shown in Table 3.

Visualization

The discovery Studio 2021 v21.1.0.20298 was used for analysis to identify 3D and 2D interactions of the complex receptor-ligand.

Table 2. Parameters for physiochemical properties.

Properties		Optical range
Lipophilicity	xLogP	-0.7–+5.0
Size	Molecular weight	150–500 g/mol
Polarity	Topological polar surface area (TPSA)	20–130
Saturation	Sp3 hybridization	Not <0.25
Flexibility	Rotatable bonds	Not more than 9

Table 3. Toxicity categorization.

Class	LD_{50} (mg/kg)
I	LD_{50} <5
II	5< LD_{50} <50
III	50< LD_{50} <300
IV	300< LD_{50} <2000
V	2000< LD_{50} <5000
VI	LD_{50} >5000

RESULTS

Selected Phytocompounds

Sixty-five phytocompounds of *C. roseus* were selected for screening from IMMPAT and their 3D structures were obtained from PubChem. Five phytocompounds were obtained with an effective binding affinity towards the BCL-6 protein, as shown in Figure 3.

Target Macromolecule and Purification of Protein

The BCL-6 gene was screened with the help of KGGE and hsa:604 was selected as a protein target. Crystal structure of the b-cell lymphoma 6 (bcl6) btb domain to 2.2 angstrom, PDB ID: 1R28 (PBD DOI: 10.2210/pdb1R28/pdb) protein model selected and downloaded in PDB file format. Purification of protein is done by BIOVIA tool where ligand and water molecules were removed, as shown in Figures 4 and 5.

Protein Structure Analysis

Secondary Structure

The 3D and secondary structure of the protein was analyzed in PDBsum. The structure has a total of 127 residues. The BCL-6 protein secondary structure has two sheets, one beta-hairpin, one psi loop, one beta bulge, four strands, seven helices, nineteen helix-helix interactions, eight beta turns, and one gamma turn, as shown in Figure 6.

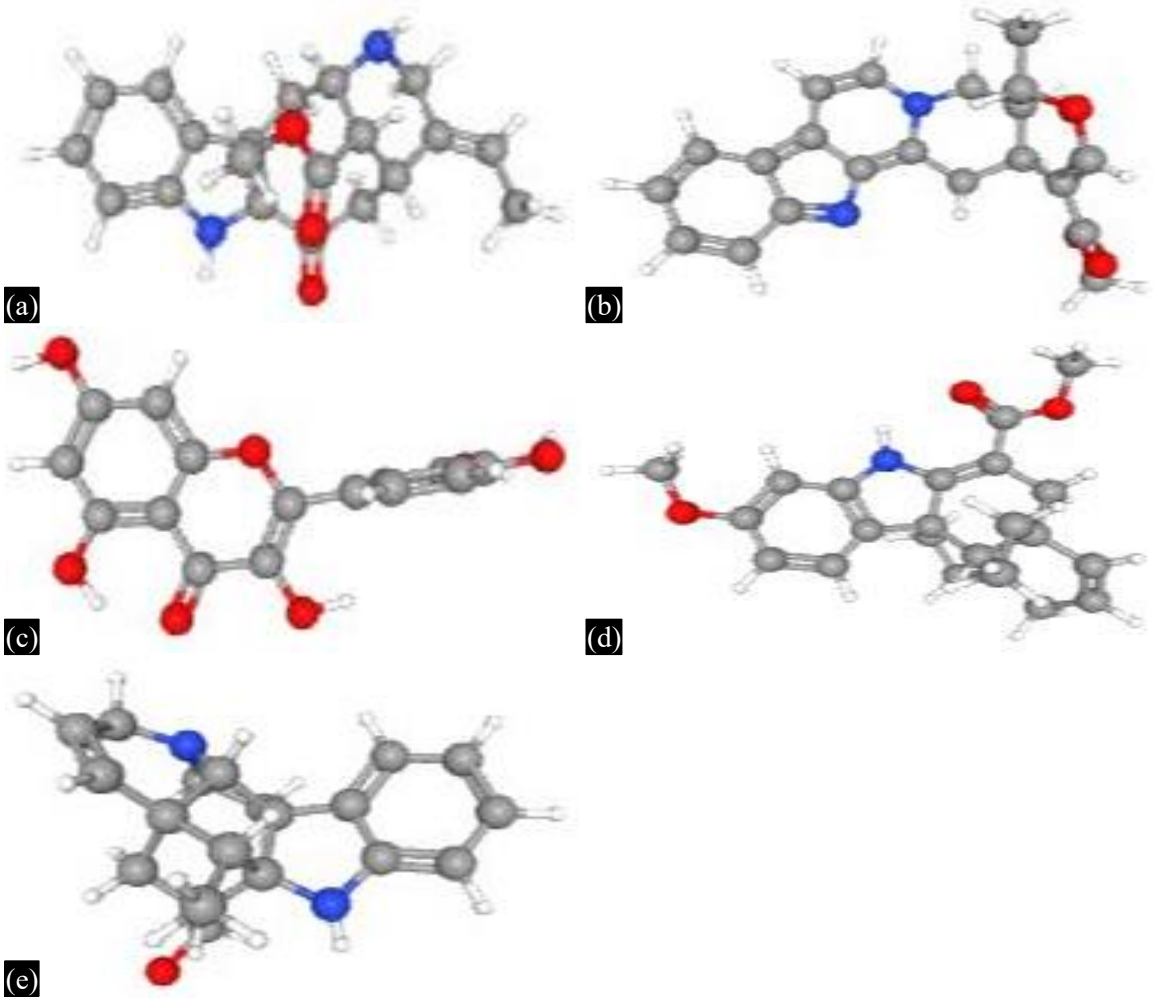

Figure 3. 3D models of selected phytocompounds from *Catharanthus roseus* (a) Perivine, (b) Alstonine, (c) Quercetin, (d) 16-Methoxytabersonine, (e) Vindolininol.

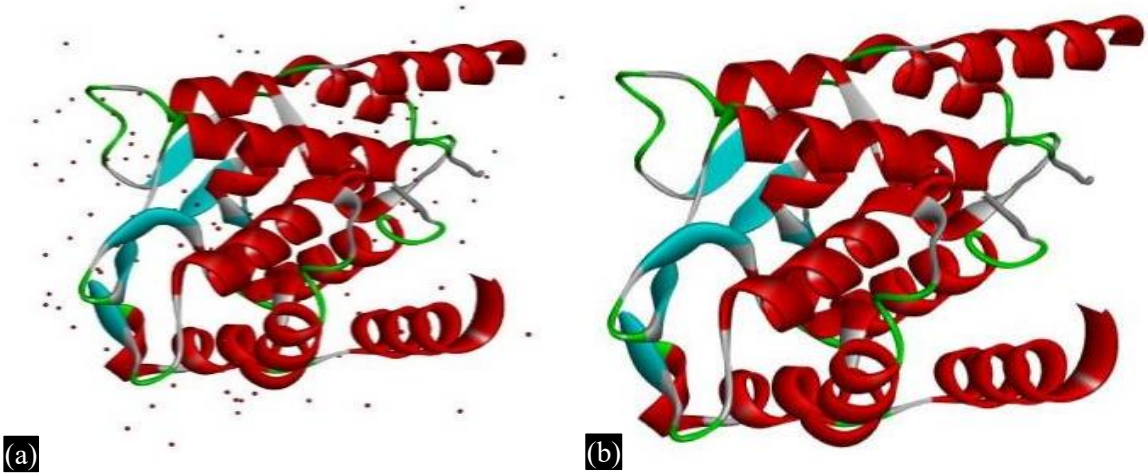

Figure 4. 3D models of BCL-6 protein obtained BIOVIA (a) 3D structure of BCL-6 protein and (b) 3D structure of purified BCL-6 protein.

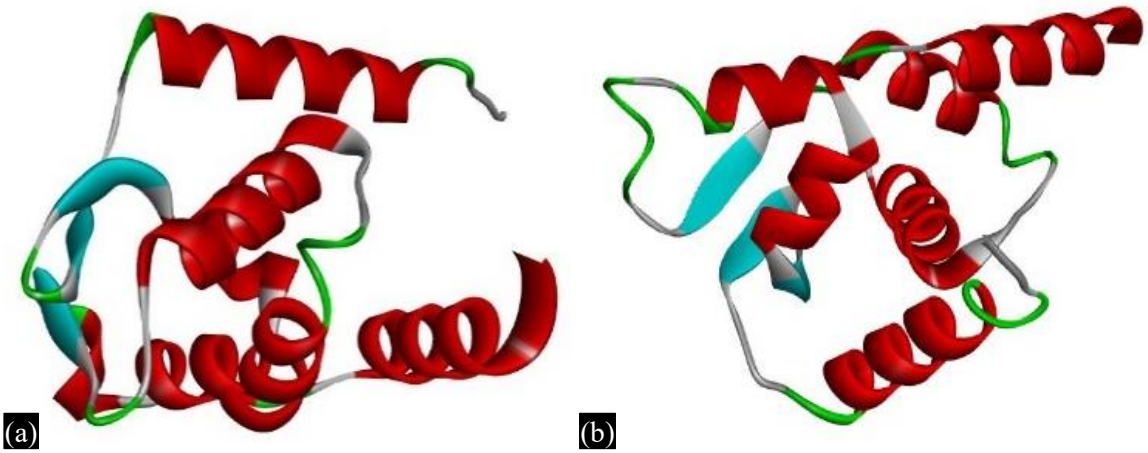

Figure 5. 3D models of purified BCL-6 protein obtained BIOVIA (a) 3D structure of purified A chain (b) 3D structure of purified B chain.

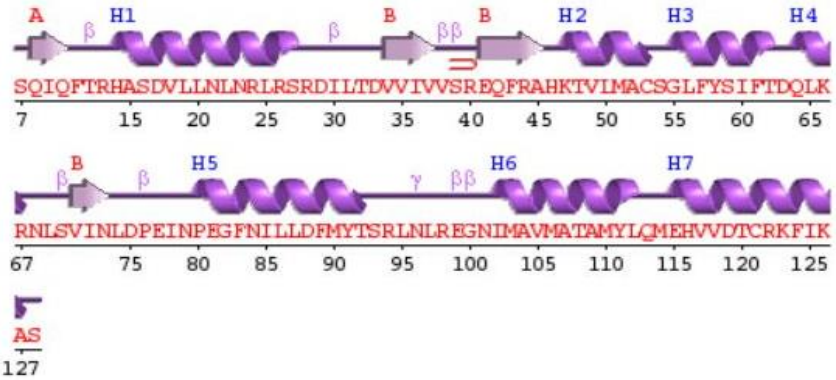

Figure 6. Secondary structure of BCL-6 protein.

Protein-Protein Interface: A}{B

In PubSum, inference statistics were obtained. The A chain has 32 interface residues, and a 1707 interface area (A^2), whereas the B chain has 28 interface residues, and a 1730 interface area (A^2). 12 hydrogen bonds interact in between chains A and B, whereas 173 non-bonded contacts. No salt bridges and disulfide bonds were found.

Ramachandran Plot

The Ramachandran plot visualized the amino acids in the energetically allowed regions based on the torsion angle ψ and Φ. In Figure 7, the Ramachandran plot was obtained using PDBsum, and PROCHECK was used. The plot statistics observed non-glycerin and non-proline 230 residues from a total of 244 residues. The plot shows red color for most favoured regions represented by A, B, L with 206 residues, additional allowed regions represented by a, b, l, p indicated yellow color with 23 residues, generously allowed regions represented by ~a, ~b, ~l, ~p in faint yellow with 0 residues, disallowed region represented by XX indicates white color with 1 residue (SER 39), the end-residues will excl. Gly and Pro 4 amino acid residues, where glycine 6 residues and proline 4 residues were analyzed in plot statistics. For the *in-silico* studies, more amino acids show in the sterically allowed region, where peptide conformation is stable.

Hydropathy Plot

EMBOSS pipwindow was used for the hydropathy plot sketched based on the hydrophobicity of amino acid; on the Y-axis hydropathy score and X-axis amino acid position were observed. Hydrophobicity shows 0 to a positive number and Hydrophilicity 0 to a negative number; where four picks above score 1 and six picks below the -1 score, as shown in Figure 8. The main purpose of the hydropathy plot is to know the hydrophobic amino acid residues align on inside, whereas hydrophilic residues on algin the outside for stability of the protein *in vivo*. High hydrophobicity protein integral into the cell membrane around 20 or more than 20 amino acid residues require into the protein. Less than 20 amino acid residues in the cell membrane were not part of it.

Protein Statistics

The protein statistics data were useful for the purification of protein and further research studies. The molecular weight of the protein is 14542.83, the average residue weight was 114.511, the charge obtained is 1.5, and the isoelectric point 7.2435. In Table 4, the protein has several non-polar, polar, and small residues, whereas in the statistical analysis obtained the number of aromatic, acidic, and basic residues. The property of amino acids, residues, their numbers, and % mole was observed by using EMBOSS pepstats.

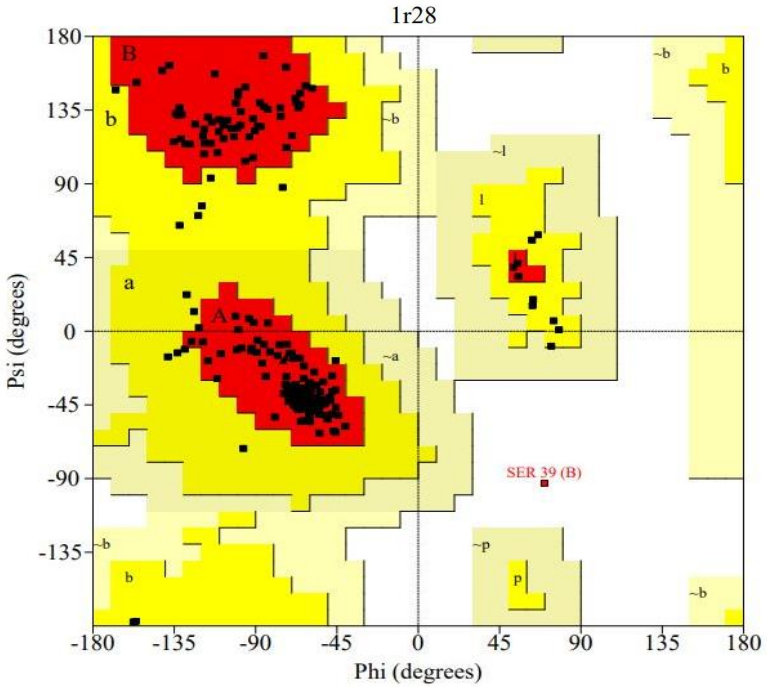

Figure 7. Ramachandran plot of BCL-6 protein.

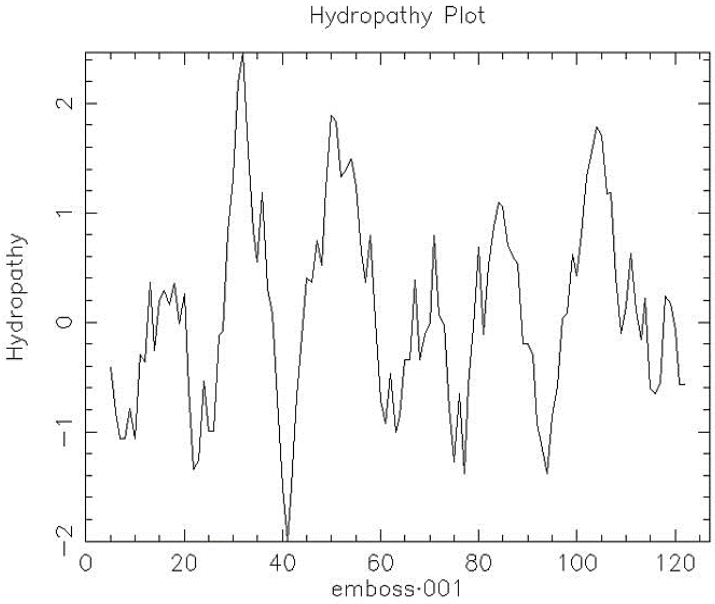

Figure 8. Hydropathy plot of BCL-6 protein obtained using EMBOSS pipwindow.

Table 4. Statistical information of BCL-6 protein by using EMBOSS pepstats.

Properties	Residues	Number	Mole %
Tiny	(A+C+G+S+T)	31	24.409
Small	(A+B+C+D+G+N+P+S+T+V)	59	46.457
Aliphatic	(A+I+L+V)	42	33.071
Aromatic	(F+H+W+Y)	13	10.236
Non-polar	(A+C+F+G+I+L+M+P+V+W+Y)	66	51.969
Polar	(D+E+H+K+N+Q+R+S+T+Z)	61	48.031
Charged	(B+D+E+H+K+R+Z)	31	24.409
Basic	(H+K+R)	17	13.386
Acidic	(B+D+E+Z)	14	11.024

Lipinski Filter Analysis

In the Lipinski analysis, 5 parameters were considered from Table 1. All ligands fit into the Lipinski parameters, except Gomaline shows a 161.03 value of molecular refractivity which is not acceptable MR must be 40-130, but the highlighted compounds in Table 5 did not follow the four minimum rules of Lipinski. Hence, it cannot be used as a candidate for drug synthesis. The Gomaline has not followed only one parameter but followed the other four parameters, so we considered it for the drug synthesis.

Pharmacological Studies

The pharmacological properties and their parameters are shown in Table 2. Table 6, all ligands fit in molecular weight. Fraction Sp3 of Kaempferol, Quercetin, Flavylium, Delphinidin, and Pelargonidin were 0 value. The saturation of Petunidin, Penonidin chloride, Hirsutidin, Rosinidin, and Malvidin was not lying in the standard parameters as not accepting less than 0.25 for saturation. The polarity of Gomaline was excluded from the 20-130 range. The lipophilicity excluded from the -0.7- +5.0 range compounds observed as Delphindin, Penonidin chloride, Cyanidin, Pelargonidin, Petunidin, Malvidin, Hirsutidin, Flavylium, and Rosinidin. Quercetin, Petunidin, Delphinidin, Pelargonidin, Cyanidin, Penonidin chloride, Flavylium, Hirsutidin, Rosinidin, Malvidin violate two of the parameters.

Table 5. Data for the properties of the Lipinski obtained using Swiss ADME.

Ligand	Formula	MW	MLOGP	H Acceptors	H donors	MR
Alstonine	$C_{21}H_{20}N_2O_3$	348.4	2.21	4	0	99.59
Resperic acid	$C_{22}H_{28}N_2O_5$	400.47	1.08	6	3	112.09
Tabernaemontanine	$C_{21}H_{26}N_2O_3$	354.44	2.13	4	1	105.4
Gomaline	$C_{30}H_{42}N_4O_2$	490.68	2.82	4	0	161.03
Perivine	$C_{20}H_{22}N_2O_3$	338.4	1.83	4	2	100.02
Kaempferol	$C_{15}H_{10}O_6$	286.24	-0.03	6	4	76.01
Quercetin	$C_{15}H_{10}O_7$	302.24	-0.56	7	5	78.03
Petunidin	$C_{16}H_{13}O_7^+$	317.27	0.03	7	5	82.66
16-Mthoxytabersonine	$C_{22}H_{26}N_2O_3$	366.45	2.7	4	1	110.95
Delphinidin	$C_{15}H_{11}ClO_7$	338.7	0.03	7	6	84.05
Pelargonidin	$C_{15}H_{11}O_5^+$	271.24	0.86	5	4	74.15
Vindolininol	$C_{20}H_{24}N_2O$	308.42	3.02	2	2	97.92
Cyanidin	$C_{15}H_{11}O_6^+$	287.24	0.32	6	5	76.17
Peonidin Chloride	$C_{16}H_{13}ClO_6$	336.72	0.81	6	4	86.49
Flavylium	$C_{15}H_{11}O^+$	207.25	3.28	1	0	66.06
Hirsutidin	$C_{18}H_{17}O_7^+$	345.32	0.52	7	3	91.6
Rosinidin	$C_{17}H_{15}O_6^+$	315.3	0.81	6	3	85.11
Coronaridine	$C_{21}H_{26}N_2O_2$	338.44	3.04	3	1	102.74
Malvidin	$C_{17}H_{15}O_7^+$	331.3	0.28	7	4	87.13
Widdrol	$C_{15}H_{26}O$	222.37	3.67	1	1	70.2
Beta-Bisabolene	$C_{15}H_{24}$	204.35	4.53	0	0	70.68
Secologanin	$C_{17}H_{24}O_{10}$	388.37	-1.95	10	4	88.04

Table 6. Physiochemical properties.

Ligand	MW	Fraction Csp3	RB	TPSA	Lipophilicity
Alstonine	348.4	0.33	2	99.59	3.33
Resperic acid	400.47	0.59	3	112.09	2.48
Tabernaemontanine	354.44	0.52	3	105.4	2.9
Gomaline	490.68	0.53	7	161.03	4.43
Perivine	338.4	0.4	2	100.02	2.73
Kaempferol	286.24	0	1	76.01	1.7
Quercetin	302.24	0	1	78.03	1.63
Petunidin	317.27	0.06	2	82.66	-2.01
16-Mthoxytabersonine	366.45	0.5	4	110.95	3.76
Delphinidin	338.7	0	1	84.05	-5.53
Pelargonidin	271.24	0	1	74.15	-2.44
Vindolininol	308.42	0.6	1	97.92	2.6
Cyanidin	287.24	0	1	76.17	-2.62
Peonidin Chloride	336.72	0.06	2	86.49	-4.64
Flavylium	207.25	0	1	66.06	-0.76
Hirsutidin	345.32	0.17	4	91.6	-0.96
Rosinidin	315.3	0.12	3	85.11	-1.01
Coronaridine	338.44	0.57	3	102.74	3.35
Malvidin	331.3	0.12	3	87.13	-1.96
Widdrol	222.37	0.87	0	70.2	3
Beta-Bisabolene	204.35	0.6	4	70.68	3.67
Secologanin	388.37	0.65	8	88.04	1.61

ADME Analysis

The BBB, GI absorption, PGB substrate, and solubility were major properties. This information was useful for the synthesis and development of drugs. The BBB restricts the compound permeation into the brain, whereas GI absorption improves the efficacy of the drug. The screening of ADME properties was obtained by using Swiss ADME in Table 7.

Toxicity Prediction

It was helpful for the prediction of the ligand toxicity based on LD_{50} (mg/kg) and toxicity class obtained by using ProTox-II in Table 8. In the test, 50% death of animals has observed after administration of the compound referred ad LD_{50}. From Table 8, Coronaridine is considered to belong to class II and should use in very less quantities may cause high toxicity.

Aggregation Data Analysis

The aggregator and non-aggregator classify the compounds by using the web server of Chem AGG. The aggregator is represented by category 1, category 0 belongs to the non-aggregator class and the score of probability supports the class of category. Non-aggregator if zero are potential lead molecules. bioavailability and synthetic solubility were also obtained in Table 9. The 0.55 or more than 0.55 of ligand shown the bioavailability score indicates the Lipinski rule of 5 was fulfilled and it depends on absorption and secretion properties. The SA score must be less than 6 (<6) to make a compound easily. The probability scores zero impossible to aggregate, whereas its potential drug candidates.

BOILED-EGG Analysis

The molecules were plotted based on legends by BOILED-EGG where Swiss ADME was used. BOILED-Egg's yolk was shown a yellow color zone predicted to passively permeate through the blood-brain barrier permeation and donated as BBB, while BOILED-Egg's white was a white color zone

Table 7. ADME data obtained using Swiss ADME.

Ligand	BBB	GI absorption	PGP substrate	Solubility (LOGSw-SILICOS IT)
Alstonine	Yes	High	No	-4.92 (Moderately soluble)
Resperic acid	No	High	No	-3.26 (Soluble)
Tabernaemontanine	Yes	High	Yes	-5.02 (Poorly soluble)
Gomaline	Yes	High	Yes	-7.14 (Moderately soluble)
Perivine	Yes	High	Yes	-5.21 (Soluble)
Kaempferol	No	High	No	-3.82 (Moderately soluble)
Quercetin	No	High	No	-3.24 (Soluble)
Petunidin	No	High	Yes	-2.77 (Soluble)
16-Mthoxytabersonine	Yes	High	Yes	-5.02 (Soluble)
Delphinidin	No	High	Yes	-2.07 (Moderately soluble)
Pelargonidin	No	High	Yes	-3.24 (Soluble)
Vindolininol	Yes	High	Yes	-4.11 (Soluble)
Cyanidin	No	High	Yes	-2.66 (Moderately soluble)
Peonidin Chloride	No	High	Yes	-3.35 (Soluble)
Flavylium	Yes	High	Yes	-5.32 (Soluble)
Hirsutidin	No	High	Yes	-4.16 (Moderately soluble)
Rosinidin	No	High	Yes	-4.05 (Moderately soluble)
Coronaridine	Yes	High	No	-5.24 (Moderately soluble)
Malvidin	No	High	Yes	-3.46 (Moderately soluble)
Widdrol	Yes	High	No	-3.63 (Soluble)
Beta-Bisabolene	No	Low	No	-3.58 (Soluble)
Secologanin	No	Low	No	1.3 (Soluble)

Table 8. Toxicity data analysis obtained using ProTox-II.

Compound	Predicted LD_{50} (mg/kg)	Predicted toxicity class
Alstonine	215	3
Resperic acid	300	3
Tabernaemontanine	2500	5
Gomaline	2000	4
Perivine	760	4
Kaempferol	3919	5
Quercetin	159	3
Petunidin	5000	5
16-Mthoxytabersonine	150	3
Delphinidin	5000	5
Pelargonidin	3919	5
Vindolininol	325	4
Cyanidin	5000	5
Peonidin Chloride	5000	5
Flavylium	2500	5
Hirsutidin	5000	5
Rosinidin	5000	5
Coronaridine	40	2
Malvidin	5000	5
Widdrol	2000	4
Beta-Bisabolene	4400	5
Secologanin	2000	4

Table 9. Aggregation data obtained using AGG.

Ligand	Aggregator class	Bioavailability score	SA score	Probability score
Alstonine	0	0.85	4.32	0.323
Resperic acid	0	0.55	4.6	0.009
Tabernaemontanine	0	0.55	4.71	0.121
Gomaline	0	0.55	3.99	0.118
Perivine	0	0.55	4.59	0.472
Kaempferol	0	0.55	3.14	0.048
Quercetin	0	0.55	3.23	0.067
Petunidin	0	0.55	3.23	0.016
16-Mthoxytabersonine	0	0.55	5.23	0.051
Delphinidin	0	0.55	3.21	0.01
Pelargonidin	0	0.55	3.04	0.015
Vindolininol	0	0.55	5.41	0.015
Cyanidin	0	0.55	3.15	0.026
Peonidin Chloride	0	0.55	3.21	0.025
Flavylium	0	0.55	2.78	0.063
Hirsutidin	0	0.55	3.47	0.02
Rosinidin	0	0.55	3.33	0.046
Coronaridine	0	0.55	4.74	0.019
Malvidin	0	0.55	3.33	0.016
Widdrol	0	0.55	4.08	0.01
Beta-Bisabolene	0	0.55	3.9	0.021
Secologanin	0	0.11	5.77	0.003

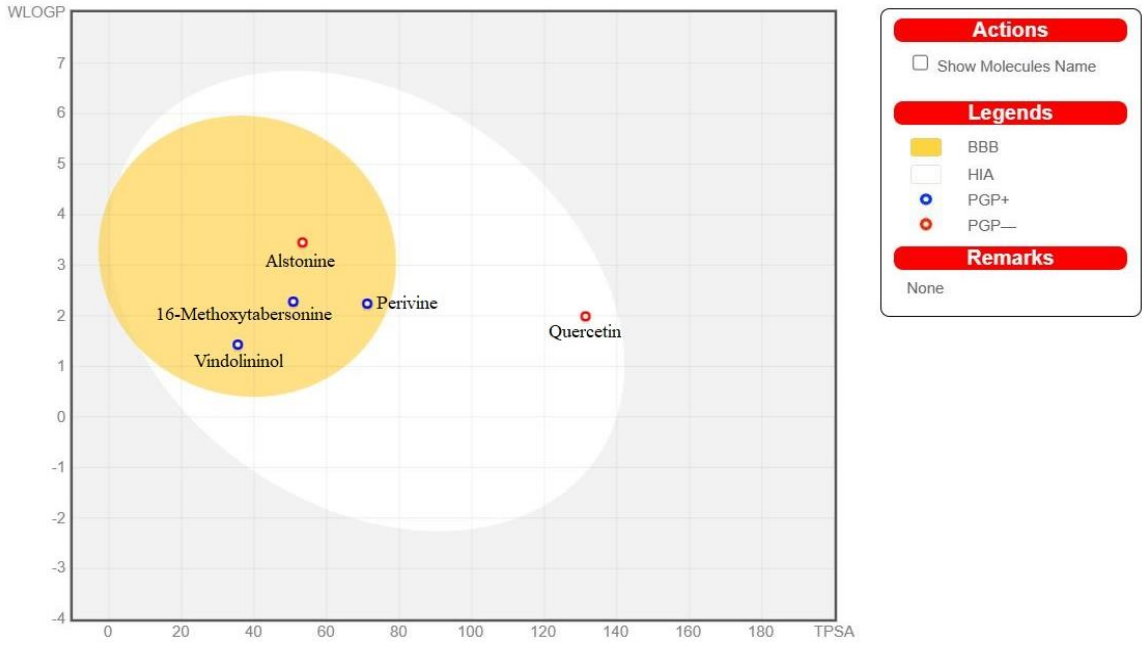

Figure 9. Brain or intestinal estimated permeation method (BOILED-EGG) diagram obtained using Swiss ADME.

predicted passively absorbed by the GI tract and denoted as HIA. The molecule predicted in the blue dot and red dot. The red dot denoted the predicted molecule effluated from the central nervous system by permeability glycoprotein (PGP+) and the blue dot denoted the predicted molecule not to be effluated from the central nervous system by the permeability glycoprotein (PGP-). The Alstonine was represented in a red dot, 16-methoxytabersonine, Vindolininol, and Perivine with a blue dot in the BOILED-Egg's yolk region. The Quercetin lies in BOILED-Egg's white with a red dot in Figure 9.

Macromolecule Structure Analysis

BCL6 is one of the important proteins of the germinal center for the differentiation of plasma cells by hyperosmotic mutation, 1R28 BCL6 screened from RCSB PDB and used as a macromolecule. The BCL6 protein consists of A and B chains, having 127 lengths of the sequence in Table 10. Three active sites were obtained by using the Prankweb server. Pocket 1 consists of 10 amino acid residues A_31, A_33, A_47, A_48, A_68, B_31, B_33, B_46, B_47, B_48, pocket 2 consists of 12 amino acid residues A_11, A_14, A_17, A_21, B_113, B_114, B_116, B_117, B_52, B_53, B_55, B_89, and pocket 3 consists of 16 amino acids residues A_113, A_114, A_115, A_116, A_117, A_51, A_52, A_53, A_54, A_55, A_89, B_11, B_13, B_14, B_17, B_21 [31]. Mutagenesis site were found A:21, A:116, B: 21, B: 116 positions concerning Uniport: P41182 for PBD 1R28 protein. The mutagenesis site abolishes interactions with NCOR2 and HDAC2, no effect on interaction with C- Terminal Binding Protein 1 (CTBP1), and transcriptional autoinhibition observed were Computed Atlas of Surface Topography of proteins (CASTp) was used for the mutagenesis site prediction [32].

Molecular Docking Analysis

As per Tables 11–13 ligands were screened for chain A, chain B, chain A and B. Twenty-two ligands were obtained from sixty-five phytocompounds of *Catharanthus roseus*. Most obtained twenty-two

Table 10. Macromolecule obtained using RCSB PDB.

Molecule	Chain	Sequence length	Organism	Details
B-cell lymphoma 6 protein	A, B	127	Homo sapiens	Mutation(s): 3 Gene Names: BCL6, BCL5, LAZ3, ZBTB27, ZNF51

Table 11. Binding affinity data for chain A obtained from PyRx.

Ligand	Binding affinity
Alstonine	-7.4
Resperic acid	-7
Gomaline	-6.5
Perivine	-6.5
Tabernaemontanine	-6.5
Kaempferol	-6.4
Quercetin	-6.3
Petunidin	-6.1
16-Mthoxytabersonine	-6.1
Delphinidin	-6.1
Pelargonidin	-6.1
Vindolininol	-6
Cyanidin	-6
Peonidin Chloride	-6
Flavylium	-5.9
Hirsutidin	-5.9
Rosinidin	-5.9
Coronaridine	-5.9
Malvidin	-5.6
Widdrol	-5.3

Table 12. Binding affinity data for chain B obtained from PyRx.

Ligand	Binding affinity
Alstonine	-6.6
Resperic acid	-6.6
Tabernaemontanine	-6.5
16-Mthoxytabersonine	-6.4
Vindolininol	-6.2
Gomaline	-6.1
Quercetin	-6.1
Kaempferol	-6.1
Pervine	-6.1
Coronaridine	-6.1
Cyanidin	-6
Delphinidin	-5.9
Pelargonidin	-5.9
Peonidin Chloride	-5.9
Petunidin	-5.9
Rosinidin	-5.9
Flavylium	-5.7
Malvidin	-5.6
Hirsutidin	-5.6
Beta-Bisabolene	-5.4

Table 13. Binding affinity data for chains A and B obtained from PyRx.

Ligand	Binding affinity
Perivine	-8
Vindolininol	-7.9
Alstonine	-7.8
16-Methoxytabersonine	-7.8
Quercetin	-7.8
Cyanidin	-7.6
Gomaline	-7.6
Coronaridine	-7.6
Tabernaemontanine	-7.5
Delphindin	-7.5
Kaempferol	-7.5
Petunidin	-7.4
Resperic acid	-7.4
Pelargonidin	-7.3
Rosinidin	-7.3
Hirsutidin	-7.2
Peonidin chloride	-7.1
Flavylium	-6.9
Malvidin	-6.8
Secologanin	-6.6

Table 14. Binding affinity data of top 5 ligands with the target protein**.**

Ligand	Binding affinity
Perivine	-8.2
Alstonine	-7.8
Quercetin	-7.8
16-methoxytabersonine	-7.8
Vindolininol	-7.8

ligands were used again for molecular docking and the best five ligands were Perivine, Alstonine, Quercetin, 16-methoxytabersonine, Vindolininol obtained and have greater binding affinity than -7.5 to the target, and use for further analysis as shown in Table 14. PyRx tool was used for molecular autodocking.

Docking of Protein with Selected Compounds

After the docking in PyRx, visualization of ligand interaction in discovery Studio 2021 v21.1.0.20298 (BIOVIA). The 2D ligand interactions were shown concerning the amino acids of the macromolecule by the van der Waals, conventional hydrogen bond, carbon-hydrogen bond, pi-donor hydrogen bond, pi-sigma, pi-pi stacked, pi-alkyl, alkyl, and unfavorable donor-donor with the specific color. The name of the amino acid with position number and chain of protein, the distance between the ligand and amino acid, category of bond, and its type for docking interactions of Perivine, Alstonine, Quercetin, 16-Methoxytabersonine, and Vindolininol were interpreted from the 2D analysis was done, as shown in Figures 10–12. The unfavorable interactional molecular docking that compounds are not a good inhibitor. The protein flexibility not taken, unexpected binding site or mode of action, solvent, entropy, and target interaction leads poorly accounted for during docking [33].

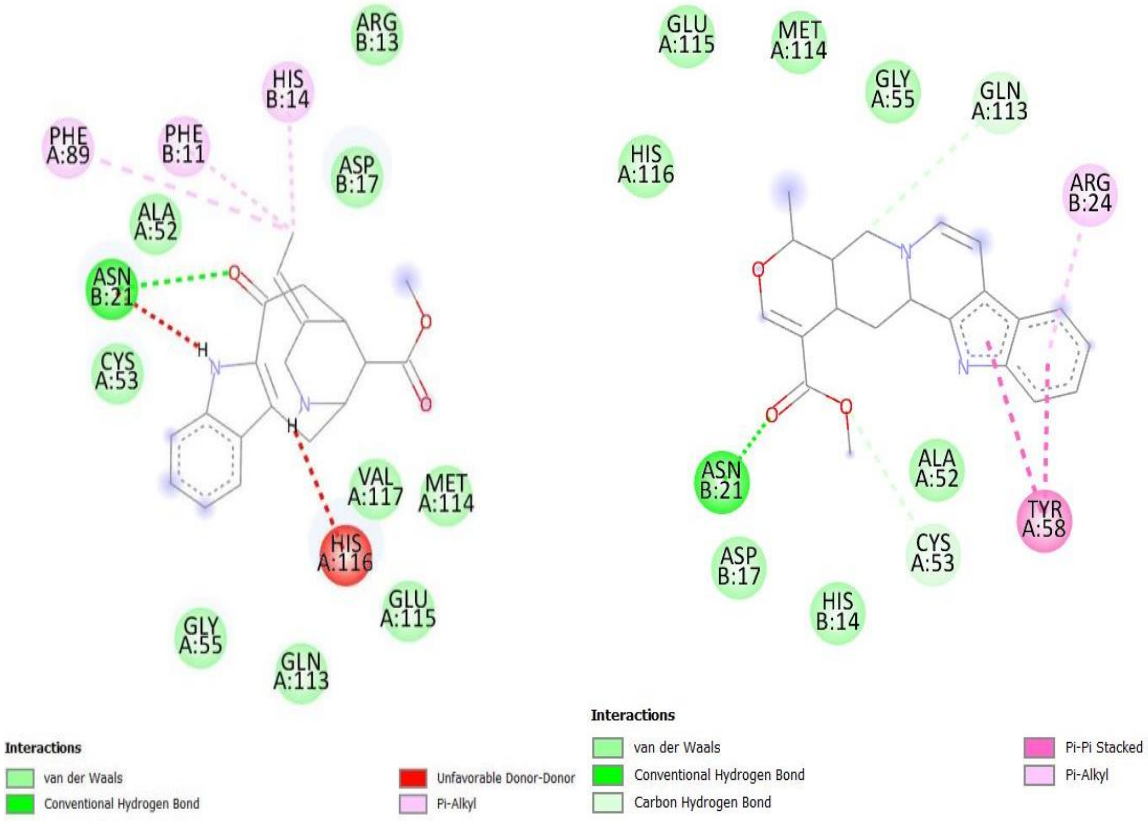

Figure 10. 2D Ligand interaction visualization of (a) Perivine and (b) Alstonine.

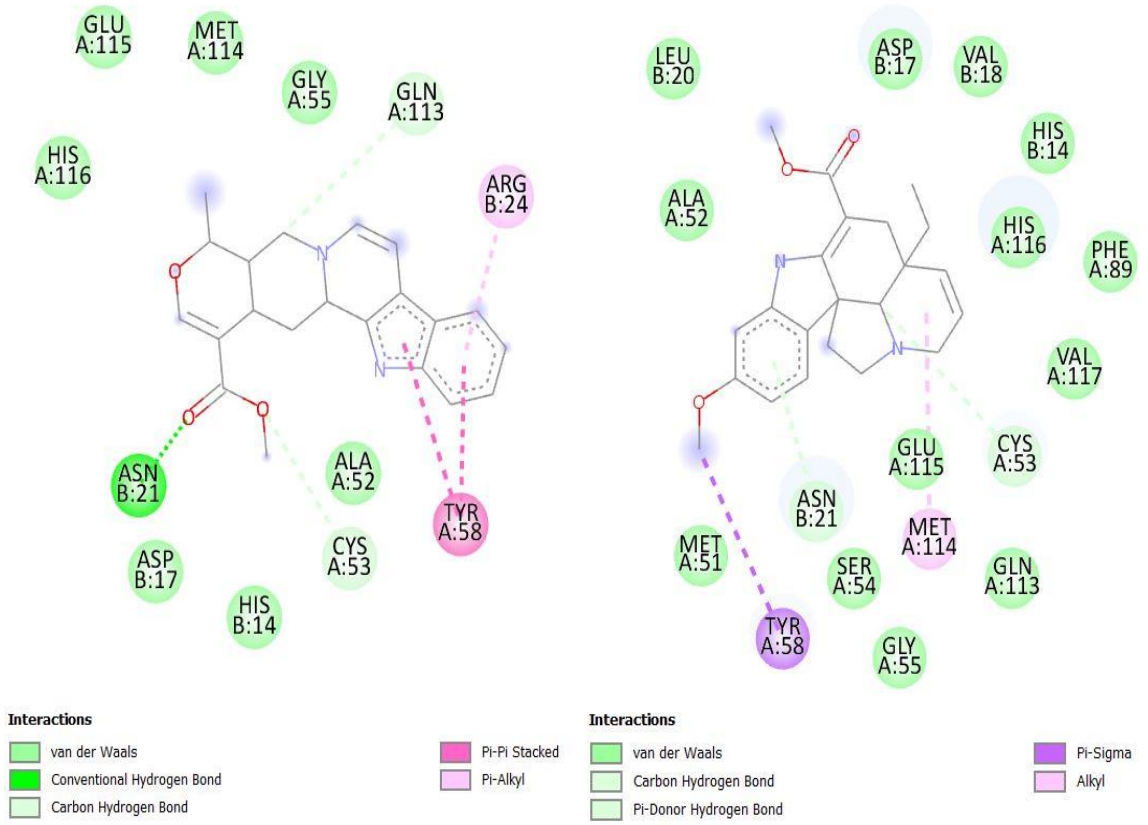

Figure 11. 2D Ligand interaction visualization of (a) Quercetin and (b) 16-Methoxytabersonine.

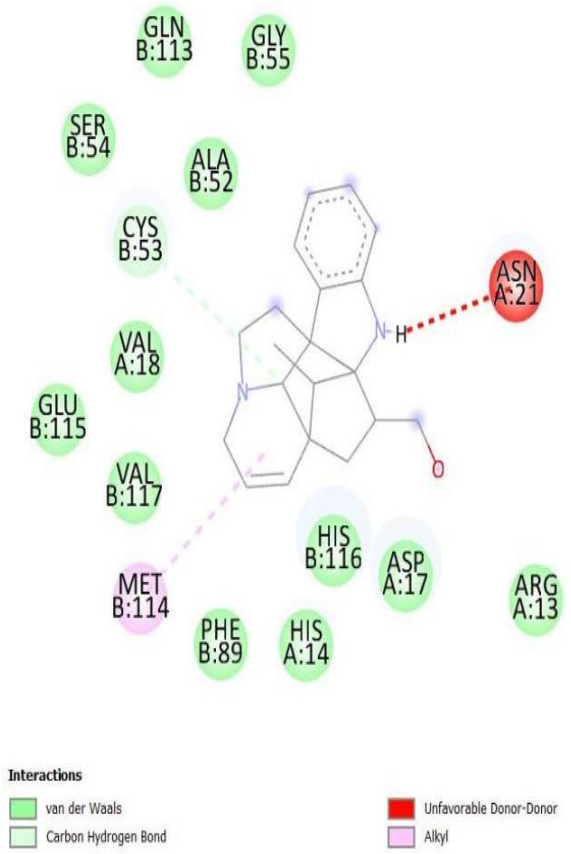

Figure 12. 2D Ligand interaction visualization of Vindolininol.

Visualization of Molecular Interaction of the Perivine with BCL6 Protein

In Tables 14 and 15, The ligand was interacting with PHE 11, HIS 14, ASN 21, PHE 89, and HIS 116 amino acids. The ligand Perivine were strong interaction with chains A and B of amino acids with a binding affinity of -8.2.

The Molecular Interaction and Visualization of the Alstonine with BCL6 Protein

In Tables 14 and 16, The ligand was interacting with ASN 21, AGR 24, CYS 53, TRY 58, and GLN 113 amino acids. The ligand Alstonine were strong interaction with chains A and B of amino acids with a binding affinity of -7.8.

The Molecular Interaction and Visualization of the Quercetin with BCL6 Protein

The ligand was interacting with ASN 21, MET 51, CYS 53, GLN 113, MET 114, GLU 115, and HIS 116 amino acids. The ligand Quercetin was a strong interaction with chains A and B of amino acids with a binding affinity of -7.8 in Tables 14 and 17.

The Molecular Interaction and Visualization of the 16-Methoxytabersonine with BCL6 Protein

The ligand was interacting with ASN 21, CYS 53, TYR 58, and MET 114 amino acids. The ligand 16-Methoxytabersonine were strong interaction with chains A and B of amino acids with a binding affinity of -7.8 in Tables 14 and 18.

The Molecular Interaction and Visualization of the Vindolininol with BCL6 Protein

The ligand was interacting with ASN 21, CYS 53, and MET 114 amino acids. The ligand Vindolininol were strong interaction with chains A and B of amino acids with a binding affinity of -7.8 in Table 14 and 19.

Table 15. Docking interactions of Perivine-protein complex.

Name	Distance	Category	Type
B: PHE 11	4.65	Hydrophobic	Pi-Alkyl
B: HIS 14	4.64	Hydrophobic	Pi-Alkyl
B: ASN 21	2.89	Hydrogen bond	Conventional hydrogen bond
B: ASN 21	2.05		Unfavorable donor-donor
A: PHE 89	5.28	Hydrophobic	Pi-Alkyl
A: HIS 116	2.39		donor-donor

Table 16. Docking interactions of Alstonine-protein complex.

Name	Distance	Category	Type
B: ASN 21	2.81	Hydrogen bond	Conventional hydrogen bond
B: AGR 24	5.41	Hydrophobic	Pi-Alkyl
A: CYS 53	3.47	Hydrogen bond	Carbon hydrogen bond
A: TRY 58	4.60 and 3.88	Hydrophobic	Pi-Pi Stacked
A: GLN 113	3.29	Hydrogen bond	Carbon hydrogen bond

Table 17. Docking interactions of Quercetin-protein complex.

Name	Distance	Category	Type
A: ASN 21	3.31	Hydrogen bond	Conventional hydrogen bond
B: MET 51	2.52	Hydrogen bond	Conventional hydrogen bond
B: CYS 53	4.66 and 3.74	Hydrophobic	Amide-pi stacked
B: GLN 113	1.85	Hydrogen bond	Conventional hydrogen bond
B: MET 114	3.39	Hydrogen bond	Carbon hydrogen bond
B: GLU 115	3.22	Hydrogen bond	Conventional hydrogen bond
B: HIS 116	3.83	Hydrogen bond	Pi-donor hydrogen bond

Table 18. Docking interactions of 16-Methoxytabersonine-protein complex

Name	Distance	Category	Type
A: ASN 21	3.80	Hydrophobic	Pi donor
A: CYS 53	3.75	Hydrogen bond	Carbon hydrogen bond
A: TYR 58	3.97	Hydrophobic	Pi-sigma
A: MET 114	5.31	Hydrophobic	Alkyl

Table 19. Docking interactions of Vindolininol-protein complex.

Name	Distance	Category	Type
A: ASN 21	2.35		Unfavorable Donor-donor
B: CYS 53	3.46	Hydrogen bond	Carbon hydrogen bond
B: MET 114	4.60	Hydrophobic	Alkyl

DISCUSSION

C. roseus phytochemicals have antimicrobial activity, cytotoxicity for the breast cancer cell line [34], antifungal activity [35], antiparasitic activity [36], anti-proliferative [37], antioxidant, and anticancer properties [38]. The lymphoma causes fevers, chills, allergies, night sweats, or unexplained weight loss greater than 10% of body weight and swelling of lymph nodes. The high rate of antibody production and other biological factors [39, 40]. Alstonine was previously used to destroy cancer cells in mice. Quercetin has anticancer effects on oesophageal cancer and acts as an apoptosis-inducing factor in vitro and in vivo [41, 42]. 16-Methoxytabersonine was previously studied as an anticancer agent, it was found in the leaf epidermis of *C. roseus*, and accumulated in the form of vindoline by biological pathway [43].

The perivine also naturally occurred into *Voacanga schweinfurthii* and *Voacanga africana*. It is an organic compound that belongs to alkaloids and derivatives with zero Lipinski rule violation. Lipinski rule was passed, and QEDw scores were 0.62. It was previously used in the *in-Vitro* study to inhibition of retinoblastoma-associated proteins (RbAP48) related to Alzheimer's disease therapy and used to treat polycystic ovarian syndrome (PCOS). Alstonine is an organic heterocyclic compound, that belongs to indol and derivatives. It naturally occurred into *Astonia constricta*, *Rauvolfia sp.*, exhibits antipsychotic activity. Lipinski's rule was passed, and QEDw scores were 0.63.

16-Methoxytabersonine is a derivative of tabersonine, an organic hetero-pentacyclic compound, monoterpenoid indol alkaloid also produced by *Alsonia yunnanesis*, *Melodinus cochinchensis*. QEDw scores were 0.66 and passed Lipinski's rule of 5. The Vindolininol is an organocyclic compound, passed Lipinski's rule of 5, and QEDw scores were 0.78. It has antimicrobial activity and inhibitors for COVID-19 from retrieving data [44]. Quercetin is a phenylpropanoid and polyketide, flavonoid, Lipinski's rule of 5 passed and QEDw scores were 0.43. It has high potential chemo-preservative activity, decreases expression of mutant p21-ras oncogene and p53 protein, and has anti-inflammatory, and anti-allergy activity [45]. It is only unfit in a fraction of sp3.

BCL6 is a transcriptional repressor with corepressors that forms the complex with other molecules and transcription is not indicated for some pathways. BCL6 is also important for plasma cell proliferation, and over-expression leads high cell proliferation rate which case B-cell lymphoma.

CONCLUSION

According to the analysis, results, and study, the *C. roseus* has Perivine, Alstonine, Quercetin, 16-Methoxytabersonine, and Vindolininol phytochemicals which have antioxidant, and anticancer, antifungal, and antiparasitic activity. In docking, these five compounds have an effective binding affinity with BCL6 and are fit for the potential drug candidate.

Acknowledgement

I hereby acknowledge the Department of Bioinformatics, BioNome, Bengaluru, India for providing computational facilities and support in the scientific research services. I thank Ms. Samiksha Bhor for their assistance throughout the project.

Funding

Nil.

ABBREVIATION

BCL: B-cell lymphoma
BBB: Blood-brain barrier
GI: Gastrointestinal
LD: Lethal dose
MR: Molecular refractivity
MW: Molecular weight
PGP: Permeability glycophorin
RB: Rotatable bond
SMILES: Simplified Molecular Input Line Entry System
SA: Synthetic accessibility
TPSA: Topological polar surface area
QEDw: Weighted quantitative estimate of drug-likeness

REFERENCES

1. Mugnaini, E. N., & Ghosh, N. (2016). Lymphoma. Primary Care: Clinics in Office Practice, 43(4), 661–675. DOI: 10.1016/j.pop.2016.07.012

2. Leeman-Neill, R. J., & Bhagat, G. (2018). BCL6 as a therapeutic target for lymphoma. Expert Opinion on Therapeutic Targets, 22(2), 143 152. DOI: 10.1080/14728222.2018.1420782
3. M. Martelli, A., Evangelisti, C., Y. Follo, M., Ramazzotti, G., Fini, M., Giardino, R., … Cocco, L. (2011). Targeting the Phosphatidylinositol 3-Kinase/Akt/Mammalian Target of Rapamycin Signaling Network in Cancer Stem Cells. Current Medicinal Chemistry, 18(18), 2715–2726. DOI: 10.2174/092986711796011201
4. Chen, L., Monti, S., Juszczynski, P., Ouyang, J., Chapuy, B., Neuberg, D., … Shipp, M. A. (2013). SYK Inhibition Modulates Distinct PI3K/AKT- Dependent Survival Pathways and Cholesterol Biosynthesis in Diffuse Large B Cell Lymphomas. Cancer Cell, 23(6), 826–838. DOI: 10.1016/j.ccr.2013.05.002
5. Isakov, N. (2018). Protein kinase C (PKC) isoforms in cancer, tumor promotion and tumor suppression. Seminars in Cancer Biology, 48, 36–52. DOI: 10.1016/j.semcancer.2017.04.012
6. Agarwal, N. K., Qu, C., Kunkulla, K., Liu, Y., & Vega, F. (2013). Transcriptional Regulation of Serine/Threonine Protein Kinase (AKT) Genes by Glioma-associated Oncogene Homolog 1. Journal of Biological Chemistry, 288(21), 15390–15401. DOI: 10.1074/jbc.m112.425249
7. Xiu, Y., Dong, Q., Fu, L., Bossler, A., Tang, X., Boyce, B., … Zhao, C. (2020). Coactivation of NF-κB and Notch signaling is sufficient to induce B-cell transformation and enables B-myeloid conversion. Blood, 135(2), 108–120. DOI: 10.1182/blood.2019001438
8. Knight, T., & Irving, J. A. E. (2014). Ras/Raf/MEK/ERK Pathway Activation in Childhood Acute Lymphoblastic Leukemia and Its Therapeutic Targeting. Frontiers in Oncology, 4. DOI: 10.3389/fonc.2014.00160
9. Abuelgasim, K. A., Shammari, R. A., Alshieban, S., Alahmari, B., Alzahrani, M., Alhejazi, A., … Damlaj, M. (2021). Impact of cluster of differentiation 20 expression and rituximab therapy in classical Hodgkin lymphoma: Real world experience. Leukemia Research Reports, 15, 100240. DOI: 10.1016/j.lrr.2021.100240
10. William, Basem & Bongu, Navneeth & Bast, Martin & Bociek, Robert & Bierman, Philip & Vose, Julie & Armitage, James. (2013). The utility of lactate dehydrogenase in the follow up of patients with diffuse large B-cell lymphoma. Revista brasileira de hematologia e hemoterapia. 35. 189-91. DOI: 10.5581/1516-8484.20130055
11. Read, K. A., Powell, M. D., Baker, C. E., Sreekumar, B. K., Ringel-Scaia, V. M., Bachus, H., … Oestreich, K. J. (2017). Integrated STAT3 and Ikaros Zinc Finger Transcription Factor Activities Regulate Bcl-6 Expression in CD4+Th Cells. The Journal of Immunology, 199(7), 2377–2387. DOI: 10.4049/jimmunol.1700106
12. Mirlekar B, Wang Y, Li S, Zhou M, Entwistle S, De Buysscher T, Morrison A, Herrera G, Harris C, Vincent BG, Ting JP, Rashid N, Kim WY, Yeh JJ, Pylayeva-Gupta Y. (2022) Balance between immunoregulatory B cells and plasma cells drives pancreatic tumor immunity. Cell Rep Med. 2022 Sep 20;3(9):100744. DOI: 10.1016/j.xcrm.2022.100744.
13. Lien, C., Fang, C.-M., Huso, D., Livak, F., Lu, R., & Pitha, P. M. (2010). Critical role of IRF-5 in regulation of B-cell differentiation. Proceedings of the National Academy of Sciences, 107(10), 4664–4668. DOI: 10.1073/pnas.0911193107
14. Zhao, S., Shen, W., Yu, J., & Wang, L. (2018). TBX21 predicts prognosis of patients and drives cancer stem cell maintenance via the TBX21–IL-4 pathway in lung adenocarcinoma. Stem Cell Research & Therapy, 9(1). DOI: 10.1186/s13287-018-0820-6
15. Chevrier, S., Kratina, T., Emslie, D., Tarlinton, D. M., & Corcoran, L. M. (2017). IL4 and IL21 cooperate to induce the high Bcl6 protein level required for germinal center formation. Immunology and Cell Biology, 95(10), 925–932. DOI: 10.1038/icb.2017.71
16. Wang, H.-Y., & Zu, Y. (2017). Diagnostic Algorithm of Common Mature B-Cell Lymphomas by Immunohistochemistry. Archives of Pathology & Laboratory Medicine, 141(9), 1236–1246. DOI: 10.5858/arpa.2016-0521-ra
17. Pillai, R. K., Sathanoori, M., Van Oss, S. B., & Swerdlow, S. H. (2013). Double-hit B-cell Lymphomas With BCL6 and MYC Translocations Are Aggressive, Frequently Extranodal Lymphomas Distinct From BCL2 Double-hit B-cell Lymphomas. The American Journal of Surgical Pathology, 37(3), 323–332. DOI: 10.1097/pas.0b013e31826cebad

18. Jaye, D., Iqbal, J., Fujita, N., Geigerman, C., Li, S., Karanam, S., … Wade, P. (2007). The BCL6-associated transcriptional co-repressor, MTA3, is selectively expressed by germinal centre B cells and lymphomas of putative germinal centre derivation. The Journal of Pathology, 213(1), 106–115. DOI: 10.1002/path.2199
19. McLachlan, T., Matthews, W. C., Jackson, E. R., Staudt, D. E., Douglas, A. M., Findlay, I. J., Persson, M. L., Duchatel, R. J., Mannan, A., Germon, Z. P., & Dun, M. D. (2022). B-cell Lymphoma 6 (BCL6): From Master Regulator of Humoral Immunity to Oncogenic Driver in Pediatric Cancers. In Molecular cancer research : MCR (Vol. 20, Issue 12, pp. 1711–1723). NLM (Medline). DOI: 10.1158/1541-7786.MCR-22-0567
20. Cortiguera, M. G., García-Gaipo, L., Wagner, S. D., León, J., Batlle-López, A., & Delgado, M. D. (2019). Suppression of BCL6 function by HDAC inhibitor mediated acetylation and chromatin modification enhances BET inhibitor effects in B-cell lymphoma cells. Scientific Reports, 9(1). DOI: 10.1038/s41598-019-52714-4
21. Das A, Sarkar S, Bhattacharyya S, Gantait S. (2020) Biotechnological advancements in Catharanthus roseus (L.) G. Don. Appl Microbiol Biotechnol. 2020 Jun;104(11):4811-4835. DOI: 10.1007/s00253-020-10592-1.
22. Bitencourt-Ferreira, G., Pintro, V. O., & de Azevedo, W. F. (2019). Docking with AutoDock4. Docking Screens for Drug Discovery, 125–148. DOI: 10.1007/978-1-4939-9752-7_9
23. Ahmad, K. F., Melnick, A., Lax, S., Bouchard, D., Liu, J., Kiang, C.-L., … Privé, G. G. (2003). Mechanism of SMRT Corepressor Recruitment by the BCL6 BTB Domain. Molecular Cell, 12(6), 1551–1564. DOI:10.1016/s1097-2765(03)00454-4
24. Riyaphan J, Pham DC, Leong MK, Weng CF. (2021). In Silico Approaches to Identify Polyphenol Compounds as α-Glucosidase and α-Amylase Inhibitors against Type-II Diabetes. Biomolecules. 2021 Dec 14;11(12):1877. DOI: 10.3390/biom11121877.
25. Madhavi Sastry, G., Adzhigirey, M., Day, T., Annabhimoju, R., & Sherman, W. (2013). Protein and ligand preparation: parameters, protocols, and influence on virtual screening enrichments. Journal of Computer-Aided Molecular Design, 27(3), 221–234. DOI: 10.1007/s10822-013-9644-8
26. Kumar S, Singh B, Singh R. (2022). Catharanthus roseus (L.) G. Don: A review of its ethnobotany, phytochemistry, ethnopharmacology and toxicities. J Ethnopharmacol. 2022 Feb 10;284:114647. DOI: 10.1016/j.jep.2021.114647
27. Long, K., Kostman, S. J., Fernandez, C., Burnett, J. C., & Huryn, D. M. (2019). Do Zebrafish Obey Lipinski Rules? ACS Medicinal Chemistry Letters, 10(6), 1002–1006. DOI: 10.1021/acsmedchemlett.9b00063
28. Shikov, A. N., Flisyuk, E. V., Obluchinskaya, E. D., & Pozharitskaya, O. N. (2020). Pharmacokinetics of Marine-Derived Drugs. Marine Drugs, 18(11), 557. doi:10.3390/md18110557
29. Dallakyan, S., & Olson, A. J. (2014). Small-Molecule Library Screening by Docking with PyRx. Chemical Biology, 243–250. DOI: 10.1007/978-1-4939-2269-7_19
30. Banerjee, P., Eckert, A. O., Schrey, A. K., & Preissner, R. (2018). ProTox-II: a webserver for the prediction of toxicity of chemicals. Nucleic Acids Research, 46(W1), W257–W263. DOI: 10.1093/nar/gky318
31. Jendele, L., Krivak, R., Skoda, P., Novotny, M., & Hoksza, D. (2019). PrankWeb: a web server for ligand binding site prediction and visualization. Nucleic Acids Research. DOI: 10.1093/nar/gkz424
32. Tian, W., Chen, C., Lei, X., Zhao, J., & Liang, J. (2018). CASTp 3.0: computed atlas of surface topography of proteins. Nucleic Acids Research, 46(W1), W363–W367. DOI: 10.1093/nar/gky473
33. Okeke, Ifeanyichukwu & Okeke, Cosmas. (2022). Molecular Docking and Analysis of In Silico Generated Ligands Against SARS-CoV-2 Spike and Replicase Proteins. 10.21203/rs.3.rs-2069911/v1.
34. Rajashekara S, Reena D, Mainavi MV, Sandhya LS, Baro U. (2022). Biological isolation and characterization of Catharanthus roseus (L.) G. Don methanolic leaves extracts and their assessment for antimicrobial, cytotoxic, and apoptotic activities. BMC Complement Med Ther. 2022 Dec 9;22(1):328. DOI: 10.1186/s12906-022-03810-y
35. Bhayana T, Gupta S. (2022). Elucidating the antifungal activity and mechanism of action of bioactive phytochemicals against fungal dermatitis isolates. Arch Dermatol Res. 2022 Nov 27. DOI: 10.1007/s00403-022-02475-4

36. Patel, S. K., Khedkar, V. M., Jha, P. C., Jasrai, Y. T., Pandya, H. A., George, L.-B., … Skelton, A. A. (2015). Molecular interaction of selected phytochemicals under the charged environment ofPlasmodium falciparumchloroquine resistance transporter (PfCRT) model. Journal of Biomolecular Structure and Dynamics, 34(2), 290–303. DOI: 10.1080/07391102.2015.1028449
37. Pham, H. N. T., Sakoff, J. A., Vuong, Q. V., Bowyer, M. C., & Scarlett, C. J. (2019). Phytochemical, antioxidant, anti-proliferative and antimicrobial properties of Catharanthus roseus root extract, saponin-enriched and aqueous fractions. Molecular Biology Reports, 46(3), 3265–3273. DOI: 10.1007/s11033-019-04786-8
38. Pham, H. N. T., Sakoff, J. A., Vuong, Q. V., Bowyer, M. C., & Scarlett, C. J. (2018). Comparative cytotoxic activity between kaempferol and gallic acid against various cancer cell lines. Data in Brief, 21, 1033–1036. DOI: 10.1016/j.dib.2018.10.121
39. Shanbhag, S., & Ambinder, R. F. (2017). Hodgkin lymphoma: A review and update on recent progress. CA: A Cancer Journal for Clinicians, 68(2), 116–132. DOI: 10.3322/caac.21438
40. Okuni M, Yakushijin K, Sakai Y, Suto H, Ichikawa H, Sakai R, Kakiuchi S, Kurata K, Mizutani Y, Kitao A, Miyata Y, Saito Y, Kawamoto S, Yamamoto K, Ito M, Matsuoka H, Minami H. (2018). A Case of Classical Hodgkin Lymphoma with Total Lymph Node Infarction. J Clin Exp Hematop. 2018 Mar 16;58(1):24-26. DOI: 10.3960/jslrt.17026
41. Davoodvandi, A., Shabani Varkani, M., Clark, C. C. T., & Jafarnejad, S. (2020). Quercetin as an anticancer agent: Focus on esophageal cancer. Journal of Food Biochemistry. DOI: 10.1111/jfbc.13374
42. Hashemzaei, M., Far, A. D., Yari, A., Heravi, R. E., Tabrizian, K., Taghdisi, S. M., … Rezaee, R. (2017). Anticancer and apoptosis-inducing effects of quercetin in vitro and in vivo. Oncology Reports, 38(2), 819–828. DOI: 10.3892/or.2017.5766
43. Qu, Y., Easson, M. L. A. E., Froese, J., Simionescu, R., Hudlicky, T., & De Luca, V. (2015). Completion of the seven-step pathway from tabersonine to the anticancer drug precursor vindoline and its assembly in yeast. Proceedings of the National Academy of Sciences, 112(19), 6224–6229. DOI: 10.1073/pnas.1501821112
44. Kalaria, Rishee & Patel, Hiren. (2020). Naturally occurring phytochemical as inhibitors from Catharanthus roseus: An In-silico approaches for drug development against COVID-19. DOI: 10.21203/rs.3.rs-116443/v1
45. Asgharian P, Tazehkand AP, Soofiyani SR, Hosseini K, Martorell M, Tarhriz V, Ahangari H, Cruz-Martins N, Sharifi-Rad J, Almarhoon ZM, Ydyrys A, Nurzhanyat A, Yessenbekova A, Cho WC. (2021) Quercetin Impact in Pancreatic Cancer: An Overview on Its Therapeutic Effects. Oxid Med Cell Longev. 2021 Nov 3;2021:4393266. DOI: 10.1155/2021/4393266

